The ascending arousal system promotes optimal performance through meso-scale network integration in a visuospatial attentional task

Authors

Gabriel Wainstein[1], Daniel Rojas-Libano[3], Dag Alnæs[3,4], Knut K. Kolskår[3, 5,6], Tor Endestad[5,7,8], Bruno Laeng[5,7], Tomas Ossandon[9,10], Nicolás Crossley[9], Elie Matar[1] and James M. Shine[1,11*]

Affiliations

1 Brain and Mind Centre, The University of Sydney, Sydney, NSW, Australia
2 Centro de Neurociencia Humana y Neuropsicología, Facultad de Psicología, Universidad Diego Portales, Santiago, Chile
3 NORMENT, Division of Mental Health and Addiction, University of Oslo, and Oslo University Hospital, Oslo, Norway
4 Bjørknes University College, Oslo, Norway
5 Department of Psychology, University of Oslo, Oslo, Norway
6 Sunnaas Rehabilitation Hospital HT, Nesodden, Norway
7 RITMO Centre for Interdisciplinary Studies in Rhythm, Time and Motion, University of Oslo, Norway
8 Helgelandssykehuset Mosjøen, Helse Nord, Norway
9 Department of Psychiatry, School of Medicine, Pontificia Universidad Católica de Chile, Santiago, Chile
10 Institute for Biological and Medical Engineering, Schools of Engineering, Medicine and Biological Sciences, Pontificia Universidad Católica de Chile, Chile
11 Centre for Complexity, The University of Sydney, Sydney, NSW, Australia

Corresponding author

* James M. Shine – mac.shine@sydney.edu.au

Abstract

There is evidence that the autonomic nervous system provides important constraints over ongoing cognitive function, however there is currently a lack of direct empirical evidence for how this interaction manifests in the brain. Here, we examine the role of ascending arousal and attentional load on large-scale network dynamics by combining pupillometry, functional MRI, and graph theoretical analysis to analyze data from a visual motion-tracking task with a parametric load manipulation. We found that attentional load effects were observable in measures of pupil diameter and in a set of brain regions that parametrically modulated their BOLD activity and meso-scale network-level integration. In addition, the regional patterns of network configuration were predicted by the distribution of the adrenergic receptor density. Our results provide confirmatory evidence for adaptive gain theory and strengthen the relationship between ascending noradrenergic tone, large-scale network integration, and cognitive task performance.

Introduction

Cognitive processes emerge from the dynamic interplay between diverse mesoscopic brain systems[1,2]. The neural activity supporting cognition does not exist in a vacuum, but instead is deeply embedded within the ongoing dynamics of the physiological networks of the body [3]. In particular, the neural processes underlying cognition are shaped and constrained by the ascending arousal system, whose activity acts to facilitate the integration between internal states and external contingencies [4]. Timely and selective interactions between the ascending arousal system and the network-level configuration of the brain are thus likely to represent crucial constraints on cognitive and attentional processes. Despite these links, we currently have a relatively poor understanding of how the ascending arousal system helps the brain as a whole to functionally reconfigure during cognitive processes, such as attention, in order to facilitate effective cognitive performance.

Recent evidence has linked higher-order functions in the brain to the intersection between whole-brain functional network architecture and the autonomic arousal system [2,5–7]. Central to this relationship is the unique neuroanatomy of the ascending noradrenergic system. For instance, the pontine locus coeruleus, which is a major hub of the ascending arousal system, sends widespread projections to the rest of the brain [8]. Upon contact, adrenergic axons release noradrenaline, which acts as a ligand on three types of post- and pre-synaptic adrenergic receptors (i.e. $\alpha 1$, $\alpha 2$ and β). The respective systemic effects of each of these receptors depend on their

differential sensitivities to noradrenaline (affinities for the ligand differ across receptors: $\alpha 2 > \alpha 1 > \beta$) and intracellular cascades, as well as their neuronal and regional distributions [8–13]. By modulating the excitability (or neural gain) of targeted regions, the locus coeruleus is thus able to effectively coordinate neural dynamics across large portions of the cerebral cortex. However, it is challenging to non-invasively track the engagement of the locus coeruleus during whole-brain neuroimaging and cognitive task performance.

Fortunately, it has been widely shown that the pupil diameter directly responds to changes in the activity of the locus coeruleus, and thus serves as an indirect, non-invasive measure of the noradrenergic system. Specifically, pupil diameter has been shown to monitor the extent to which ongoing neural activity is sensitive to inputs from regions that are structurally connected to the locus coeruleus [14,15]. In addition, fast, phasic changes in pupil diameter directly relate to changes in the activity of the locus coeruleus [16–18]. While there is some evidence that pupil dilation covaries with other subcortical systems [19], there is also clear causal evidence linking stimulation of the locus coeruleus to dilation of the pupil [20,21]. This suggests that the pupil can be used as an indirect, non-invasive measure of the ascending noradrenergic arousal system.

There are demonstrated links between cognitive processes, whole-brain network architecture, and the ascending arousal system. For instance, both physical and mental effort have previously been linked to activity within the ascending arousal system [22,23]. In addition, sympathetically-mediated dilations in pupil diameter have been shown to effectively track the allocation of attentional resources [24–26]. Despite these insights, several questions remain unanswered regarding how these processes are related to the complex architecture of the brain [27]. For instance, the processes by which the ascending arousal system modulates the functional dynamics of brain networks to facilitate attention, decision making and optimal performance, have only begun to be explored [21,28–30].

To examine these relationships in more detail, participants performed a motion-tracking task (top panel of Figure 1A) involving four levels of increasing attentional load while simultaneous BOLD fMRI and pupillometry data were collected. Subjects were instructed to covertly track the movement of a number of pre-identified targets (two to five) in a field of non-target stimuli (ten in total, including targets; see Figure 1). The attentional load was modulated through the manipulation of the number of

items a participant was required to covertly attend to over the 11s tracking period. We hypothesized that, if increasing mental effort led to the reconfiguration of large-scale network architecture via the ascending arousal system, then the number of items required to be tracked over time (i.e., the attentional load) should relate to: i) increased pupil diameter; ii) heightened BOLD activity within attentional networks; and iii) augmented topological integration. Also, we predicted that individual differences in pupil diameter should track with individual differences in effective attentional performance and decision processes [30–32]. Finally, we tested if the regional patterns of network configuration were predicted by the distribution of a predefined adrenergic receptor density atlas [21,29,33,34]. Our results confirm these predictions, and hence provide a mechanistic link between network topology, ascending noradrenergic arousal and attentional load.

Methods

Participants

18 right-handed individuals (age 19–26 years; 5 male) were included in this study. Exclusion criteria included: standard contraindications for MRI; neurological disorders; mental disorders or drug abuse. All participants gave written informed consent before the experiment.

Parametric Motion Tracking Task

Each trial of the task involved the same basic pattern (Figure 1A): the task begins with a display presenting the objects (i.e., blue colored disks); after a 2.5 s delay, a subset of the disks turns red for another 2.5 seconds; all of the disks then return to blue (2.5 seconds) before they started moving randomly inside the tracking area. The participants' job is to track the 'target' dots on the screen while visually fixating at the cross located at the center of the screen. After a tracking period of ~11 seconds, one of the disks is highlighted in green (a 'probe') and the subject is then asked to respond, as quickly as possible, as to whether the green probe object was one of the original target objects. The number of objects that subjects were required to attend to across the tracking period varied across trials. There were five trial types: passive viewing (PV), in which no target are assigned; and four load conditions, in which two to five targets were assigned for tracking. We operationalized attentional load as the linear effect of increasing task difficulty (i.e., the number of targets to be tracked).

The experiment was conducted using a blocked design, in which each block included: instruction (1s); fixation (0.3s, present throughout the rest of trial); object

presentation (all objects were blue; 2.5s); target assignment (i.e., the targets changed color from blue to red; 2.5s); object representation (objects back to the original blue color; 2.5s); object movement/attentional tracking (moving blue dots; 11s); object movement cessation (0.5s); and a final probe (color change to green and response; 2.5 s). The total duration of each trial was 22.8s. Each condition was repeated 4 times in one fMRI-run, which also included 4 separate fixation periods of 11s each between five consecutive trials. All participants completed 4 separate runs of the experiment, each of which comprised 267 volumes. The order of the conditions was pseudo-random, such that the different conditions were grouped in sub-runs of triplets: PV, pseudo-random blocks of Loads 2 through 5 and a fixation trial. All objects were identical during the tracking interval and standard object colors were isoluminant (to minimize incidental pupillary responses during the task).

Behavior and EZ-Diffusion Model

To analyse the effect of load on tracking and to account for the sample size (i.e., 16 trials for each condition within subject), we performed a bootstrapping analysis [35] in which we randomly resampled (500 times) each attentional load condition to calculate the mean value for accuracy and reaction time (RT) [36,37] and the standard deviation of the RT (SD-RT). After this step, we performed a linear regression with task load as a predictor and then performed a t-test on the β regressors from the first level analysis (see Results).

In addition, an EZ-diffusion model was used to interpret the performance measures from the task [38,39]. This model considers the mean RT of correct trials, SD-RT across correct trials, and mean accuracy across the task and computes from these a value for drift rate (ν), boundary separation (α), and non-decision time (T_{er}) – the three main parameters for the drift-diffusion model [38,40]. For each term, the mean of the resampled distribution was analysed for linear dependencies with attentional load.

Pupillometry

Fluctuations in pupil diameter of the left eye were collected using an MR-compatible coil-mounted infrared EyeTracking system (NNL EyeTracking camera, NordicNeuroLab, Bergen, Norway), at a sampling rate of 60 Hz and recorded using the iView X Software (SensoMotoric Instruments, SMI GmbH, Germany). Blinks, artifacts and outliers were removed and linearly interpolated [41]. High frequency noise was smoothed using a 2nd order 2.5 Hz low-pass Butterworth filter. To obtain

the pupil diameter average profile for each level of attentional load (Fig. 1B), data from each participant was normalized across each task block. This allowed us to correct for low frequency baseline changes without eliminating the load effect and baseline differences due to load manipulations [42,43].

Time-Resolved Functional Connectivity and Network Analysis

Details for MRI data collection and preprocessing are present in the Supplementary Materials. Following pre-processing, the mean time series was extracted from 375 predefined regions-of-interest (ROI). To estimate functional connectivity between the 375 ROIs, we used the Jack-knife correlation approach (JC) [44]. Time-resolved adjacency matrices were then subjected to topological analysis following a protocol defined in previous work [2] – see Supplementary Materials for details.

Neurotransmitter Receptor Mapping

To investigate the potential correlates of meso-scale integration, we interrogated the neurotransmitter receptor signature of each region of the brain. We used the Allen Brain Atlas micro-array atlas (http://human.brain-map.org/) to identify the regional signature of genetic expression of two subtypes of adrenergic receptor (ADRA1A and ADRA2A) that have been *a priori* related to cognitive function and attention [45], and are the most abundant adrenergic subtypes expressed in the cerebral cortex [46]. To test for specificity, we also evaluated two muscarinic receptor densities (Chrm1 and Chrm2) and two dopaminergic receptor densities (Drd1 and Drd2).

Linear model

To evaluate the effect of the density of each receptor on meso scale integration, we built a linear model aimed at predicting integration. Previous work has shown the effect of glutamatergic release and neuromodulation on integration [47], and that BOLD activity is closely related to glutamatergic release [48]. We therefore used the mean BOLD activity during tracking, and the interaction effect of BOLD to the receptor density (to account for the role of activation on integration) for each of the cortical regions, as predictors, and participation as the model's outcome. The deterministic part of the model is expressed in the following equation using Wilkinson notation [49]:

$$PC \sim BOLD + BOLD:\alpha 1a + BOLD:\alpha 2a + 1$$

Where PC is meso-scale participation coefficient; BOLD is the average BOLD activity during tracking for each region; α1a and α2a are the regional densities of the respective adrenergic receptor; BOLD: α1a and BOLD: α2a measures the interaction between the terms on the PC.

We fitted the model to individual subject data, and then analyzed both the mean effect across subjects (t-test), as well as the relationship between model parameters and pupillometry results.

Results

The Relationship Between Sympathetic Tone and Attentional Processing

Consistent with previous work [5], our bootstrapping analysis (see methods) found that task performance (i.e., correct responses) decreased with attentional load (mean β_{Acc} = -0.05; $t_{(17)}$ = -4.81, p = 2.0x10^{-4}; Figure S1B) and RT (mean β_{RT} = 0.06, $t_{(17)}$ = 5.19, p = 7.2x10^{-5}). We expanded on this result by translating performance into EZ-diffusion model parameters [39,50], wherein we observed a decrease in both the boundary criteria (α; β_{Bound} = -7.8x10^{-3}, $t_{(17)}$ = -2.86, p = 0.011) and drift rate (ν; mean β_{Drift} = -0.03, $t_{(17)}$ = -4.22, p = 6.0x10^{-4}; Figure 1B), and an increase in the non decision time (mean β_{nondec} = 0.04, $t_{(17)}$ = 2.15, p = 0.045) with increasing attentional load.

By calculating the linear effect of load on pupil size across a moving average window of 160ms (see Methods), we observed a main effect of increased pupil diameter across both the tracking and probe epochs ($\beta_{pupil} > 0$, $p_{FDR} < 0.01$; light grey in Figure 1A depict significant epochs of time during the task; and in Figure S1A show the group average β_{pupil} time series) and a positive correlation between the mean drift rate and accuracy across all load conditions to pupil dilation during the significant period (i.e., the light grey area in Figure 1A; r_{drift} = 0.77, p = 2.0x10^{-4}; Figure 1C; Pearson r_{acc} = 0.8, p = 7.0x10^{-5}, Figure S1C). The same relationships were not observed with T_{er} (r_{Ter} = -0.19, p = 0.44) nor boundary (r_{α} = 0.437, p = 0.70). These results suggest that attentional load manipulation and pupil dilation covaried with performance on this attentionally demanding task [2].

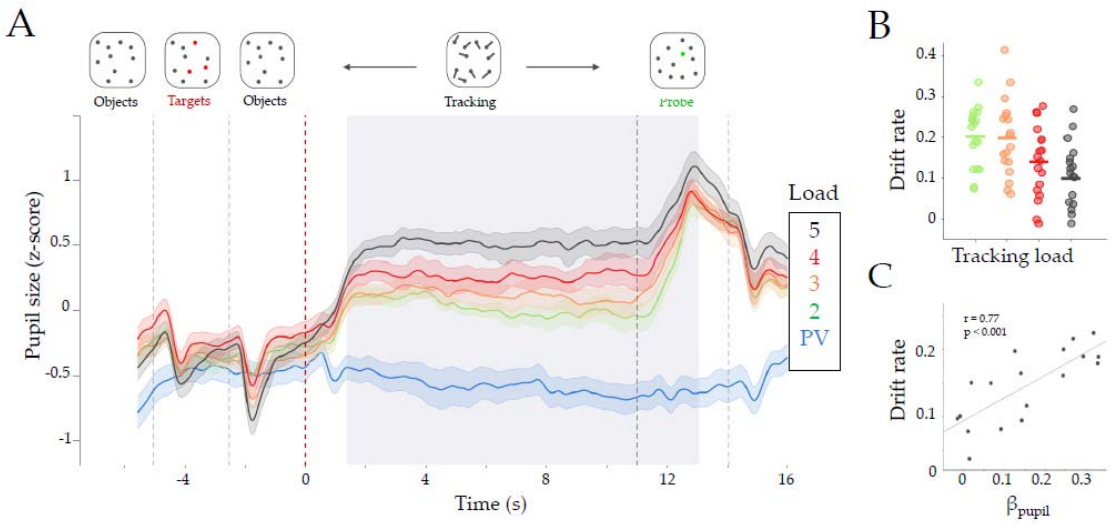

Figure 1: Effect of task difficulty on pupil diameter. A) Group average (z-score) pupil diameter time series for each Load condition. Colors represent passive viewing (PV) in blue, and Load 2 to 5 in green, orange, red and black, respectively. The shaded area represents the standard error of the mean. We observed an average increase in pupil diameter, during tracking, with each Load condition. Light grey area represents the significant effect ($\beta_{pupil} > 0$; FDR corrected at $p < 0.01$). Dotted lines represent the onset of each trial event (showed in the top part of the Figure). The red dotted line (Time = 0) is the tracking onset period when the dots began to move; B) Drift rate in each load condition. Each dot is the average drift rate for each subject and load (mean β_{Drift} = -0.03, $t_{(17)}$ = -4.22, p = 6.0x10^{-4}); C) Pearson correlation between the pupil parametric effect of Load (β_{pupil}) with the average drift rate across subjects (r_{drift} = 0.77, p = 2.0x10^{-4}). The x-axis is the mean beta estimate of the pupillary load effect of the significative time window (β_{pupil}) and the y-axis represents the mean drift rate across Loads.

Network Integration Increases as a Function of Attentional Load

Based on previous studies, we hypothesized that an increase in attentional load should recruit a distributed functional network architecture [5] and also heighten network integration [2,11,29]. To test this hypothesis, we implemented a hierarchical topological network analysis [51–53] to the time-resolved functional connectivity average, specifically during the tracking period of the task. Our analysis identified a subnetwork of tightly inter-connected regions that were part of a diverse attentional, somatomotor, and cerebellar networks (red in Figure 2) that increased its BOLD activity after the tracking onset (Figure 2F). The tightly integrated regions were diversely connected to a separate frontoparietal sub-module (blue in Figure 2) that was less active during the trial. The remaining two sub-modules (yellow and green in Figure 2) showed a negative BOLD response during the tracking period and were part of a diverse set of networks. Interestingly, 81% of the Frontoparietal network (FPN) and all the Default Mode Network (DMN) were found to be within this less

active group (see Supplementary Table S1 for the complete list of regions and sub-module assignments).

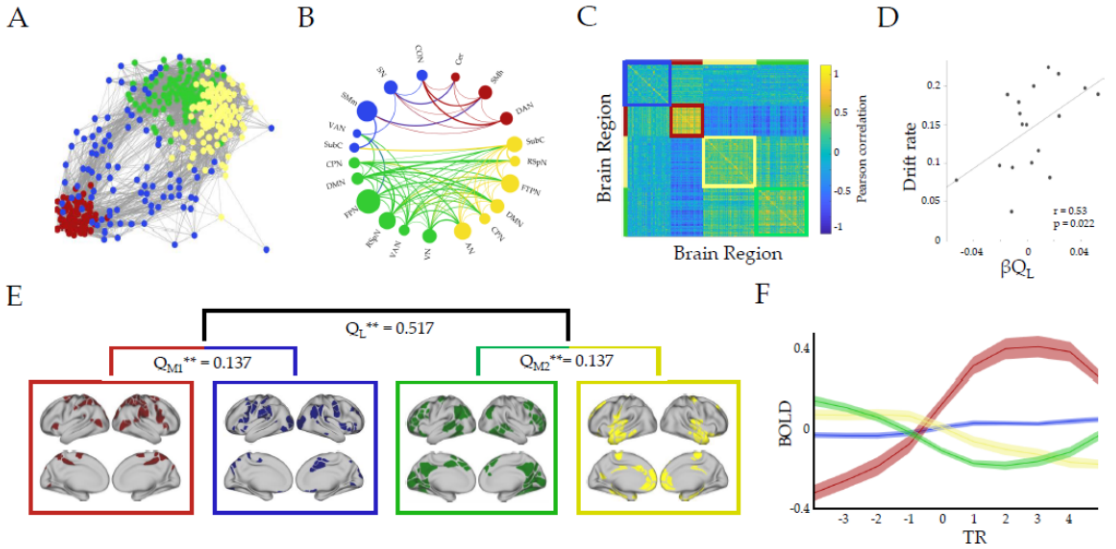

Figure 2: Hierarchical functional topology analysis of the brain during tracking across all loads. We observed two large-scale modules, and two meso-scale modules within each larger module (Module one [M1, red/blue] and Module two [M2, green/yellow], respectively): M1 corresponded to predominantly attentional and somatomotor networks, and M2 to Frontoparietal (FPN) and Default Mode Network (DMN) among others (B and E). A) Forced directed plot representation of the average cluster across subjects. Each color represents a unique sub module; B) A circle plot representing the resting state regions that were included within each sub module, with networks with > 30% of regions in each submodule shown in the plot. The diameter of the circles corresponds to the percentage of network regions that participated in that cluster. Connection width relates to average positive connection strength (functional connectivity), however only connections with r > 0.1 are shown; C) Connectivity matrix (Pearson's r) between all pair of regions ordered by module assignments – note the strong anti-correlation between the red and green/yellow sub-modules; D) Correlation between parametric load effect on large scale modularity (β_Q value), and drift rate (r = 0.53; p = 0.022); E) Hierarchical analysis representation: Q_L, Q_{M1} and Q_{M2} represent the modularity value for each level (Q_L large scale, and $Q_{M1\text{-}M2}$ meso-scale level) and ** represents the probability of finding this value when running a null model (p = 0). The brain maps correspond to the cortical regions associated with each sub module; F) BOLD mean effect for each sub-cluster, each line represents the group average, and shaded areas are the standard error of the mean, x-axis is Repetition Time (TR) centered around tracking onset (TR = 0). DAN, dorsal attention; VN, visual; FPN, frontoparietal; SN, salience; CO, cingulo-opercular; VAN, ventral attention; SMm, somatomotor mouth; SMh, somatomotor hand; RSpN, retrosplenial; FTP, frontotemporal; DMN, default mode; AN, auditory; CPN, cinguloparietal; SubC, subcortex; Cer, Cerebellar.

Contrary to expectations, we did not observe significant parametric topological change at the macroscopic level as a function of attentional load (p > 0.05 for all TRs, Figure S2A). Indeed, when analysing the correlation between modularity and

performance measures (i.e., accuracy, drift rate and pupil diameter), we observed that an increase in the large scale modularity parametric effect (i.e., higher segregation with load, β_{QL}) positively correlated with higher drift rate (r = 0.53; p = 0.022; Figure 2D), accuracy (r = 0.61; p = 0.007; Supplementary Figure S3A), but was independent from pupil diameter (r = 0.43; p = 0.073). These results suggested that the system reconfigured during tracking towards increasing modularity (i.e., large scale segregation), which in turn affected the efficient encoding of the ongoing task during tracking and hence, the decision making process during the task probe.

Upon closer inspection of the data (Figure 2C), we observed a substantial number of nodes playing an integrative role during task performance. Specifically, the red sub-module was found to selectively increase its participation coefficient (PC) at the meso-scale level (i.e., by connecting to the blue submodule) as a function of increasing attentional load (β_{PC} = 2.4x10^{-3}, $F_{(1,\ 70)}$ = 5.79; p = 0.019; Figure 3A). Additionally, the extent of integration in the red sub-module was positively correlated across subjects with pupil diameter (Pearson r = 0.62, p = 0.006; Figure 3B), drift rate (Pearson's r = 0.66, p = 0.002; Figure 3C) and accuracy (r = 0.57, p = 0.012, Figure S3B). Importantly, these relationships were found to be specific to the red sub-module. Thus, although the macroscale network did not demonstrate increased integration *per se*, the relative amount of meso-scale integration within the red community was associated with increased performance (i.e., drift rate) and sympathetic arousal (i.e., pupil diameter). In this way, these results provide a direct relationship between the effect of attention load on pupillometry, drift rate, and a trade-off between large-scale segregation and meso-scale network integration.

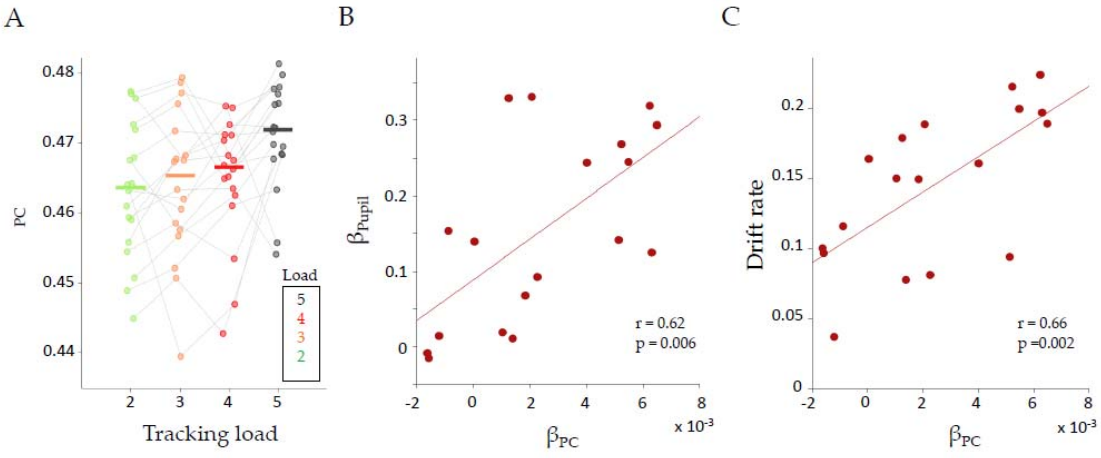

Figure 3: Relationships between load effect on participation, drift rate and pupil load effect. A) Average participation coefficient (PC) for each load, for the red module, during tracking. Each color represents the corresponding tracking load (from 2 to 5). Grey lines correspond to each subject; B-C)

A regression parameter (β_{PC}) was calculated for each subject and then correlated to β_{pupil} (B; r = 0.62; p = 0.006) and Drift rate (C; r = 0.66; $p = 2.4x10^{-3}$). Each circle corresponds to the mean value per subject.

Network meso-scale integration and adrenergic receptor density

Given the physiological determinants of pupil diameter, the results of our analyses strongly suggested that the adrenergic system is involved in these processes of meso-scale network reconfiguration. Importantly, the direct effect of the locus coeruleus directly depends on the presence of noradrenergic receptors. There are three classes of receptors (i.e., α1, α2, and β receptors), two of which (α1a, α2a) have previously been associated with working memory, adaptive gain and attention [12,54,55]. Importantly, they have differentiated effects based both on different intracellular cascades, different sensitivities to noradrenaline [12,54] and differential distribution across the cortex and neuronal circuitry [56,57]. Thus, these receptors seem to play distinct roles during cognition, specifically in processes in which the ascending attentional system is implicated [9,10]. To gain a deeper insight about adrenergic receptors' role in the process, we extracted the regional expression of ADRA1A and ADRA2A genes from the Allen Human Brain Atlas repository [58,59], which encode for α1a and α2a adrenoceptors, respectively, and compared the regional expression of these two genes with the meso-scale communities identified (Figure 2E).

We hypothesized that, if pupil diameter is a readout of the noradrenergic system, which in turn is acting to shape and constrain meso-scale functional network architecture, then the different modules and sub-modules that we observed should have different densities of neuromodulatory receptors. We indeed observed significant differences between modules at each hierarchical level (ADRA1A – between large-scale modules: $T_{(331)} = 0.33$, $p = 0.736$, $p_{perm} = 0.736$; Within red/blue: $T_{(135)} = 2.09$, $p = 0.038$, $p_{perm} = 0.038$; Within green/yellow: $T_{(194)} = -3.31$, $p = 0.001$, $p_{perm} = 0.001$; ADRA2A – between large-scale modules: $T_{(331)} = -3.00$, $p = 0.003$, $p_{perm} = 0.003$; Within red/blue: $T_{(135)} = -1.40$, $p = 0.164$, $p_{perm} = 0.167$; Within green/yellow: $T_{(194)} = 3.82$, $p = 0.0002$, $p_{perm} = 0.002$; Figure 4A-B).

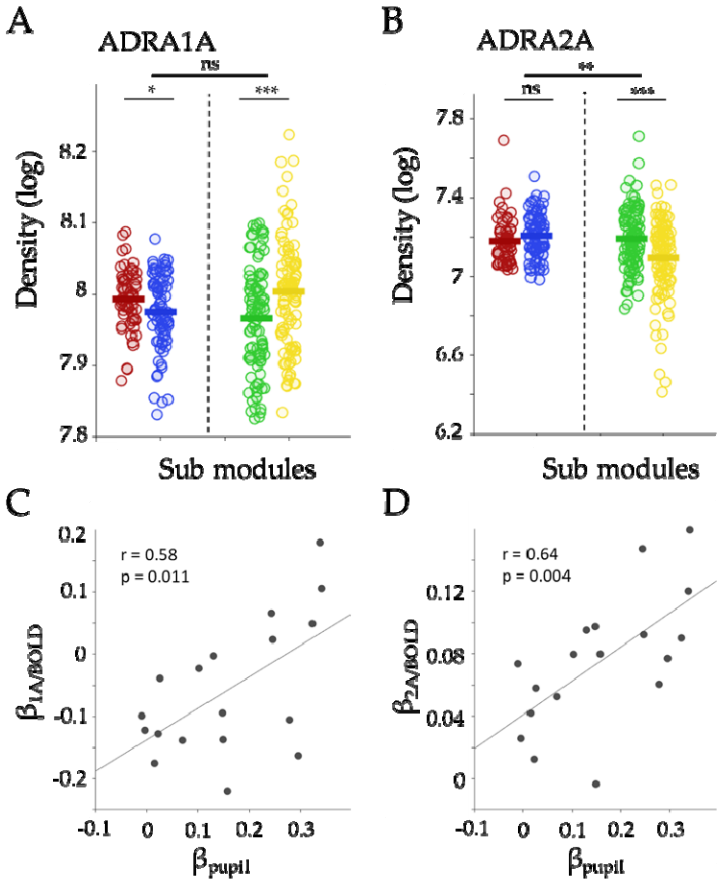

Figure 4: Receptor density analysis. The density of the ADRA1A and ADRA2A receptor expression, for each of the sub modules is shown in A and B, respectively. In each hierarchical level (i.e. at the largescale and mesoscale) it is shown the permuted t-test results with significance levels: ^{ns} $p > 0.05$; * $p < 0.05$ ** $p < 0.01$; *** $p < 0.001$. C-D). C-D) Pearson correlation between the model β estimate ($\beta_{1A/BOLD}$ and $\beta_{2A/BOLD}$, respectively) and pupil diameter (β_{pupil}). Colors as in figure 2.

The modulatory effects of noradrenaline have been argued to depend directly on ongoing glutamatergic activity on the target region [47]. Given the differential task-related BOLD activity of the different sub-modules (Figure 2D), and the observed regional variability and specificity of integration across the network, we hypothesized that network-level integration would be well explained by the intersection between the distribution of the adrenergic receptor expression and the BOLD activity of individual cortical regions, which putatively represents pooled neural spiking activity [60]. To evaluate this hypothesis, we created a linear model that used average BOLD activity during tracking and its interaction with adrenergic receptor expression to explain meso-scale network participation (See Methods). The model was fit at the subject-level, and both the mean effect across subjects, as well as the relationship between model fits and β_{pupil} were analyzed. Across subjects, we

observed a positive interaction between BOLD and α2a ($\beta_{2A/BOLD}$ = 0.08, $T_{(17)}$ = 7.57; $p < 1.0x10^{-4}$, $p_{Perm} = 3.0x10^{-4}$), while neither α1a ($\beta_{1A/BOLD}$ = -0.06, $T_{(17)}$ = -2.22, p = 0.039; p_{Perm} = 0.140), nor BOLD (β_{BOLD} = -0.06, $T_{(17)}$ = -0.23, p = 0.817, p_{Perm} = 0.540) survived 100,000 non-parametric permutations that scrambled the regions mesoscale participation coefficient (i.e. the dependent variable in the model). In contrast, the correlation between the model parameters and β_{pupil} revealed a positive correlation for both adrenergic receptors (r_{ADRA1A} = 0.58, p = 0.011; r_{ADRA2A} = 0.64, p = 0.004; Figure 4C-D) and a negative correlation for β_{BOLD} (r_{BOLD} = -0.60, p = 0.004).

We confirmed the specificity of this result by repeating the linear regression analysis with the regional densities of m1 and m2 cholinergic receptors (encoded by Chrm1 and Chrm2 genes, respectively), and D1 and D2 dopaminergic receptors (encoded by Drd1 and Drd2 genes, respectively), which are receptors from two separate neuromodulatory systems involved in attention, working memory and network functional dynamics. Although both neuromodulatory systems related to meso-scale integration (M1: $\beta_{M1/BOLD}$ = 0.08, $T_{(17)}$ = 5.73, $p < 1.0x10^{-4}$; D1: $\beta_{D1/BOLD}$ = 0.07, $T_{(17)}$ = 8.04; $p < 1.0x10^{-4}$; Supplementary Table S2 for the complete regression results), neither of the subjects respective regressors correlate with β_{pupil} (p was greater than 0.500 for all correlations), meaning that the change of the regressor across subjects (i.e., the effect of the receptor on regional integration) and its relation to pupil diameter is specific of the adrenergic receptors studied here (Figure 4C-D).

Discussion

Here, we leveraged a unique dataset to simultaneously track pupil diameter and network topology during an attentional demanding task with increasing attentional load. Our results provide integrative evidence that links the ascending arousal system to the mesoscale topological signature of the functional brain network during the processing of an attentionally demanding cognitive task. Pupil diameter tracked with attentional load (Figure 1A) and was related to the speed of information accumulation as estimated by a drift diffusion model (Figure 1B-C). Additionally, we observed concurrent pupil dilations and adaptive mesoscale parametric topological changes as a function of task demands (Figures 2 and 3). Finally, we found evidence that topological reconfiguration was dependent on the intersection between BOLD activity and the genetic expression of the adrenergic receptors in the brain (Figure 4). Together, these results provide evidence for the manner in which the ascending arousal noradrenergic system reconfigures brain network topology so as to promote attentional performance according to task demands.

The relationship between performance and pupil diameter is consistent with the predictions of Adaptive Gain Theory [15]. Within this framework, the locus coeruleus is proposed to adaptively alter its activity according to the demands imposed on the system. More specifically, the theory proposes that performance follows an inverted U-shaped relationship with arousal, such that maximal operational flexibility in the noradrenergic system is associated with optimal task performance [12,55]. We observed that load-related increases in pupil diameter, presumably due to increased activity in the ascending arousal system [15,17,61], relates closely with the activity and topology of the broader brain network (Figure 2), in a manner that is reflective of effective task performance (Figure 3). Similar effects have been described in animal models after a chemogenetic activation of the locus coeruleus, which strongly alters the large-scale network structure towards large-scale integration, specifically in regions with heightened adrenergic receptor expression [21]. How these changes, which are likely related to the modulation of the neural gain that mediates effective connections between distributed regions of the brain [28], are traded-off against requirements for specificity and flexibility remains an important open question for future research.

The addition of attentional load was found to alter the integration of meso-scale sub-modules, but not the higher-level modular organization. This topological result is somewhat more targeted than those described in previous work [2,29,62]. While these differences may be related to disparities in the way that the data were analyzed, the results of our study do demonstrate that alterations in the cerebral network topology at a relatively local (i.e., sub-modular) level are crucial for effective task performance[63]. Additionally, our results replicate and expand upon a previous study [64], in which the authors found that short term practice on an attentional task was related to increased coupling between attentional networks and segregation among task-negative (DMN) and frontoparietal network (FPN). Our study replicates the graph theoretical results of that study, while also directly relating the findings to the architecture of the ascending neuromodulatory system. One potential explanation for these results comes from animal studies, in which rapid changes in pupil diameter have been compared to changes in neural population activity at the microscale [17,65,66]. These studies suggest that the ascending arousal system may be able to alter the topology of the network in a hierarchical manner that is commensurate with the spatiotemporal scale of the arousal systems' capacity [2]. Future work that integrates results across

spatiotemporal scales is required to appropriately adjudicate the implications of this hypothesis.

In summary, we provide evidence linking mesoscale topological network integration, hierarchical organization and BOLD dynamics in the human brain to increases in attentional load, thus providing further mechanistic clarity over the processes that underpin the Adaptive Gain Model of noradrenergic function in the central nervous system.

Funding and Disclosure

JMS was supported by the University of Sydney Robinson Fellowship and NHMRC GNT1156536. GW was supported by 'Becas Chile' Phd scholarship. The authors declare no financial interests or conflicts of interest.

Author Contributions

GW and JS Analysed the data, interpreted the results and wrote the manuscript. DR: Interpreted the results and wrote the manuscript. KK, DA, BL and TE: Created the experimental design and contributed with the data acquisition. All authors reviewed, commented and edited the manuscript, and all authors gave final approval of the version to be published.

References

1. Shine JM. The thalamus integrates the macrosystems of the brain to facilitate complex, adaptive brain network dynamics. Prog Neurobiol. 2020:101951.
2. Shine JM, Bissett PG, Bell PT, Koyejo O, Balsters JH, Gorgolewski KJ, et al. The Dynamics of Functional Brain Networks: Integrated Network States during Cognitive Task Performance. Neuron. 2016;92:544–554.
3. Varela F, Lachaux J-P, Rodriguez E, Martinerie J. The brainweb: phase synchronization and large-scale integration. Nat Rev Neurosci. 2001;2:229–239.
4. Parvizi J, Damasio A. Consciousness and the brainstem. Cognition. 2001;79:135–160.
5. Alnæs D, Sneve MH, Espeseth T, Endestad T, van de Pavert SHP, Laeng B. Pupil size signals mental effort deployed during multiple object tracking and predicts brain activity in the dorsal attention network and the locus coeruleus. J Vis. 2014;14:1–20.
6. Shine JM, Hearne LJ, Breakspear M, Hwang K, Müller EJ, Sporns O, et al. The low-dimensional neural architecture of cognitive complexity is related to activity in medial thalamic nuclei. Neuron. 2019;104:849–855.
7. Alnæs D, Kaufmann T, Richard G, Duff EP, Sneve MH, Endestad T, et al. Attentional load modulates large-scale functional brain connectivity beyond the core attention networks. Neuroimage. 2015;109:260–272.
8. Samuels E, Szabadi E. Functional Neuroanatomy of the Noradrenergic Locus Coeruleus: Its Roles in the Regulation of Arousal and Autonomic Function Part II:

Physiological and Pharmacological Manipulations and Pathological Alterations of Locus Coeruleus Activity in Humans. Curr Neuropharmacol. 2008;6:254–285.
9. Bouret S, Sara SJ. Network reset: A simplified overarching theory of locus coeruleus noradrenaline function. Trends Neurosci. 2005;28:574–582.
10. Sara SJ. The locus coeruleus and noradrenergic modulation of cognition. Nat Rev Neurosci. 2009;10:211–223.
11. Shine JM. Neuromodulatory Influences on Integration and Segregation in the Brain. Trends Cogn Sci. 2019;23:572–583.
12. Robbins TW, Arnsten AFT. The neuropsychopharmacology of fronto-executive function: monoaminergic modulation. Annu Rev Neurosci. 2009;32:267–289.
13. Aston-Jones G, Waterhouse B. Locus coeruleus: From global projection system to adaptive regulation of behavior. Brain Res. 2016;1645:75–78.
14. van den Brink RL, Pfeffer T, Warren CM, Murphy PR, Tona K-D, van der Wee NJA, et al. Catecholaminergic neuromodulation shapes intrinsic MRI functional connectivity in the human brain. J Neurosci. 2016;36:7865–7876.
15. Aston-Jones G, Cohen JD. An integrative theory of locus coeruleus-norepinephrine function: adaptive gain and optimal performance. Annu Rev Neurosci. 2005;28:403–450.
16. Murphy PR, Boonstra E, Nieuwenhuis S. Global gain modulation generates time-dependent urgency during perceptual choice in humans. Nat Commun. 2016;7:1–15.
17. Joshi S, Li Y, Kalwani RM, Gold JI. Relationships between Pupil Diameter and Neuronal Activity in the Locus Coeruleus, Colliculi, and Cingulate Cortex. Neuron. 2016;89:221–234.
18. Reimer J, Froudarakis E, Cadwell CR, Yatsenko D, Denfield GH, Tolias AS. Pupil Fluctuations Track Fast Switching of Cortical States during Quiet Wakefulness. Neuron. 2014;84:355–362.
19. Joshi S, Gold JI. Pupil Size as a Window on Neural Substrates of Cognition. Trends Cogn Sci. 2020;24:466–480.
20. Liu Y, Rodenkirch C, Moskowitz N, Schriver B, Wang Q. Dynamic lateralization of pupil dilation evoked by locus coeruleus activation results from sympathetic, not parasympathetic, contributions. Cell Rep. 2017;20:3099–3112.
21. Zerbi V, Floriou-Servou A, Markicevic M, Vermeiren Y, Sturman O, Privitera M, et al. Rapid reconfiguration of the functional connectome after chemogenetic locus coeruleus activation. Neuron. 2019;103:702–718.
22. Mulder G. The Concept and Measurement of Mental Effort. Energ Hum Inf Process. 2012:175–198.
23. Varazzani C, San-Galli A, Gilardeau S, Bouret S. Noradrenaline and Dopamine Neurons in the Reward/Effort Trade-Off: A Direct Electrophysiological Comparison in Behaving Monkeys. J Neurosci. 2015;35:7866–7877.
24. Gilzenrat MS, Nieuwenhuis S, Jepma M, Cohen JD. Pupil diameter tracks changes in control state predicted by the adaptive gain theory of locus coeruleus function. Cogn Affect Behav Neurosci. 2010;10:252–269.
25. Wainstein G, Rojas-Líbano D, Crossley NA, Carrasco X, Aboitiz F, Ossandón T. Pupil size tracks attentional performance in attention-deficit/hyperactivity disorder. Sci Rep. 2017;7:1–9.
26. Kahneman D, Beatty J. Pupil Diameter and Load on Memory. Science. 1966;154:1583–1585.

27. Shenhav A, Musslick S, Lieder F, Kool W, Griffiths TL, Cohen JD, et al. Toward a Rational and Mechanistic Account of Mental Effort. Annu Rev Neurosci. 2017;40:99–124.
28. Shine JM, van den Brink RL, Hernaus D, Nieuwenhuis S, Poldrack RA. Catecholaminergic manipulation alters dynamic network topology across cognitive states. Netw Neurosci. 2018;2:381–396.
29. Shine JM, Breakspear M, Bell PT, Ehgoetz Martens K, Shine R, Koyejo O, et al. Human cognition involves the dynamic integration of neural activity and neuromodulatory systems. Nat Neurosci. 2019;22:289–296.
30. de Gee JW, Colizoli O, Kloosterman NA, Knapen T, Nieuwenhuis S, Donner TH, et al. Dynamic modulation of decision biases by brainstem arousal systems. Elife. 2017;6:e23232.
31. Donner T, Kettermann A, Diesch E, Ostendorf F, Villringer A, Brandt SA. Involvement of the human frontal eye field and multiple parietal areas in covert visual selection during conjunction search. Eur J Neurosci. 2000;12:3407–3414.
32. de Gee JW, Knapen T, Donner TH. Decision-related pupil dilation reflects upcoming choice and individual bias. Proc Natl Acad Sci. 2014;111:E618–E625.
33. Fornito A, Arnatkevičiūtė A, Fulcher BD, Fornito A, Arnatkevi A. Bridging the gap between connectome and transcriptome. Trends Cogn Sci. 2019;23:34–50.
34. Richiardi J, Altmann A, Milazzo A-C, Chang C, Chakravarty MM, Banaschewski T, et al. Correlated gene expression supports synchronous activity in brain networks. Science. 2015;348:1241–1244.
35. Wilcox RR, Rousselet GA. A Guide to Robust Statistical Methods in Neuroscience. Curr Protoc Neurosci. 2018;82:8.42.1-8.42.30.
36. Whelan R. Effective analysis of reaction time data. 2008:475–482.
37. Rousselet GA, Wilcox RR. Reaction times and other skewed distributions: Problems with the mean and the median. BioRxiv. 2018:1–26.
38. Ratcliff R, Rouder J. Modeling response times for two-choice decisions. Psychol Sci. 1998;9:347–356.
39. Wagenmakers EJ, Van Der Maas HLJ, Grasman RPPP. An EZ-diffusion model for response time and accuracy. Psychon Bull Rev. 2007;14:3–22.
40. Ratcliff R, Smith PL, Brown SD, Mckoon G. Diffusion decision model: Current issues and history. Trends Cogn Sci. 2016;20:260–281.
41. Wainstein G, Rojas-Líbano D, Crossley NA, Carrasco X, Aboitiz F, Ossandón T. Pupil size tracks attentional performance in attention-deficit/hyperactivity disorder. Sci Rep. 2017;7:1–9.
42. Rojas-Líbano D, Wainstein G, Carrasco X, Aboitiz F, Crossley N, Ossandón T. A pupil size, eye-tracking and neuropsychological dataset from ADHD children during a cognitive task. Sci Data. 2019;6:25.
43. Campos-Arteaga G, Forcato C, Wainstein G, Lagos R, Palacios-García I, Artigas C, et al. Differential neurophysiological correlates of retrieval of consolidated and reconsolidated memories in humans: an ERP and pupillometry study. Neurobiol Learn Mem. 2020:107279.
44. Thompson WH, Richter CG, Plavén-Sigray P, Fransson P. Simulations to benchmark time-varying connectivity methods for fMRI. PLoS Comput Biol. 2018;14:1–23.
45. Arnsten AFT, Haven N. The Neurobiology of Thought : The Groundbreaking Discoveries of Patricia Goldman-Rakic 1937 – 2003. 2013:2269–2281.

46. Perez DM. α1-Adrenergic Receptors in Neurotransmission, Synaptic Plasticity, and Cognition. Front Pharmacol. 2020;11:1–22.
47. Mather M, Clewett D, Sakaki M, Harley CW. Norepinephrine ignites local hotspots of neuronal excitation: How arousal amplifies selectivity in perception and memory. Behav Brain Sci. 2016;39.
48. Betina Ip I, Berrington A, Hess AT, Parker AJ, Emir UE, Bridge H. Combined fMRI-MRS acquires simultaneous glutamate and BOLD-fMRI signals in the human brain. Neuroimage. 2017;155:113–119.
49. Wilkinson GN, Rogers CE. Symbolic Description of Factorial Models for Analysis of Variance. J Appl Stat. 1973;22:392–399.
50. Ratcliff R, Thompson CA, McKoon G. Modeling individual differences in response time and accuracy in numeracy. Cognition. 2015;137:115–136.
51. Meunier D, Lambiotte R, Bullmore ET. Modular and hierarchically modular organization of brain networks. Front Neurosci. 2010;4:1–11.
52. Meunier D, Lambiotte R, Fornito A, Ersche KD, Bullmore ET. Hierarchical modularity in human brain functional networks. Front Neuroinform. 2009;3:1–12.
53. Bassett DS, Greenfield DL, Meyer-lindenberg A, Weinberger DR, Moore SW, Bullmore ET. Efficient physical embedding of topologically complex information processing networks in brains and computer circuits. PLoS Comput Biol. 2010;6:e1000748.
54. Wang M, Ramos BP, Paspalas CD, Shu Y, Simen A, Duque A, et al. α2A-adrenoceptors strengthen working memory networks by inhibiting cAMP-HCN channel signaling in prefrontal cortex. Cell. 2007;129:397–410.
55. Arnsten AFT, Wang MJ, Paspalas CD. Neuromodulation of Thought: Flexibilities and Vulnerabilities in Prefrontal Cortical Network Synapses. Neuron. 2012;76:223–239.
56. Santana N, Artigas F. Laminar and cellular distribution of monoamine receptors in rat medial prefrontal cortex. Front Neuroanat. 2017;11:1–13.
57. Zilles K, Palomero-gallagher N. Multiple Transmitter Receptors in Regions and Layers of the Human Cerebral Cortex. 2017;11:1–26.
58. Hawrylycz MJ, Lein ES, Guillozet-bongaarts AL, Shen EH, Ng L, Miller JA, et al. An anatomically comprehensive atlas of the adult human brain transcriptome. Nature. 2012;489:391–399.
59. Gryglewski G, Seiger R, James GM, Godbersen GM, Komorowski A, Unterholzner J, et al. Spatial analysis and high resolution mapping of the human whole-brain transcriptome for integrative analysis in neuroimaging. Neuroimage. 2018;176:259–267.
60. Logothetis NK. The Underpinnings of the BOLD Functional Magnetic Resonance Imaging Signal. 2003;23:3963–3971.
61. Liu Y, Rodenkirch C, Moskowitz N, Schriver B. Dynamic Lateralization of Pupil Dilation Evoked by Locus Coeruleus Activation Results from Article Dynamic Lateralization of Pupil Dilation Evoked by Locus Coeruleus Activation Results from Sympathetic , Not Parasympathetic , Contributions. CellReports. 2017;20:3099–3112.
62. Shine JM, Aburn MJ, Breakspear M, Poldrack RA. The modulation of neural gain facilitates a transition between functional segregation and integration in the brain. Elife. 2018;7:e31130.
63. Akiki TJ, Abdallah CG. Determining the Hierarchical Architecture of the Human Brain Using Subject-Level Clustering of Functional Networks. Sci Rep. 2019;9:1–15.

64. Mohr H, Wolfensteller U, Betzel RF, Mišić B, Sporns O, Richiardi J, et al. Integration and segregation of large-scale brain networks during short-term task automatization. Nat Commun. 2016;7:1–12.
65. Reimer J, Froudarakis E, Cadwell CR, Yatsenko D, Denfield GH, Tolias AS. Pupil Fluctuations Track Fast Switching of Cortical States during Quiet Wakefulness. Neuron. 2014;84:355–362.
66. McGinley MJ, Vinck M, Reimer J, Batista-Brito R, Zagha E, Cadwell CR, et al. Waking State: Rapid Variations Modulate Neural and Behavioral Responses. Neuron. 2015;87:1143–1161.